ACS OMEGA

Open Access

http://pubs.acs.org/journal/acsodf

Article

Harnessing Microbial Effectors for Macrophage-Mediated Drug Delivery

Anton Du Preez Van Staden,* Johan G. Visser, Yigael S. L. Powrie, and Carine Smith*

Cite This: *ACS Omega* 2024, 9, 18260−18272

Read Online

ACCESS | Metrics & More | Article Recommendations | Supporting Information

ABSTRACT: Macrophage-based drug delivery systems are promising, but their development is still in its infancy, with many limitations remaining to be addressed. Our aim was to design a system harnessing microbial effectors to facilitate controlled drug cargo expulsion from macrophages to enable the use of more toxic drugs without adding to the risk of off-target detrimental effects. The pore forming and actin polymerizing *Listeria monocytogenes* effectors listeriolysin-O (LLO) and actin assembly-inducing protein (ActA) were synthesized using a novel green fluorescent protein (GFP)-linked heterologous expression system. These effectors were coated onto polystyrene beads to generate "synthetic cargo" before loading into primary M1 macrophages. Bead uptake and release from macrophages were evaluated by using high-throughput quantitative imaging flow cytometry and confocal microscopy. *In vitro* results confirmed appropriate activity of synthesized effectors. Coating of these effector proteins onto polystyrene beads (simulated drug cargo) resulted in changes in cellular morphology, bead content, and intracellular bead localization, which may support an interpretation of the induced release of these beads from the cells. This forms the basis for further investigation to fully elucidate any potential release mechanisms. Bacterial effectors ActA and LLO successfully effectuated actin polarization and protrusions from cell membranes similar to those seen in cells infected with *Listeria* spp., illustrating the potential of using these effectors and production methods for the development of an endogenous drug delivery system capable of low-risk, targeted release of high potency drugs.

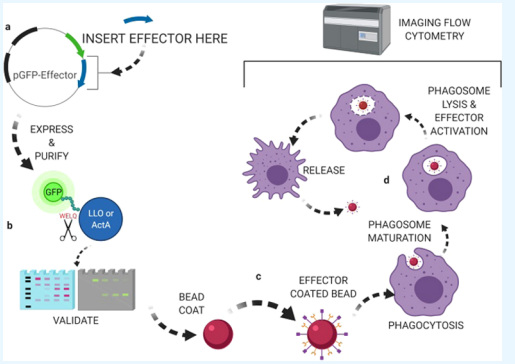

INTRODUCTION

Given their central role in inflammation, macrophages, as well as macrophage membranes and macrophage-derived vesicles, have become popular components of cell-based drug delivery systems in the context of several conditions characterized by inflammation. As recently reviewed,[1] particular advantages of macrophage-based systems—especially when paired with nanoparticle technology—are the prolongation of drug half-life and circulation time, reduced immunogenicity, and improved targeting ability.

The unique properties of the macrophage membrane allow sustained, slow release of drugs,[2−7] which may improve the pharmacokinetic properties of drugs where a requirement exists for sustained therapeutic levels, for example, as recently described in the context of rheumatic disease management.[8] However, in instances where drugs with higher toxicity need to be delivered, for example, in drug-resistant infections or even chemotherapy, a more targeted approach is desirable to reduce undesired off-target effects. There is thus room for the development of a drug delivery system, which combines unique macrophage properties—such as transmembrane migratory capacity to reach target sites,[9,10] their endogenous targeting capacity,[11−15] and the known anti-inflammatory effect facilitated by macrophage membranes[16,17] and a mechanism by which the timing of drug release may be controlled.

We have been developing such a system (Figure 1), with the consideration of key aspects that should be incorporated in the system design. First, drug stability in transit should be optimized. One of the most commonly used techniques for drug loading into macrophages is simply incubation to achieve loading via endocytic processes such as phagocytosis. However, due to the harsh phagosomal environment, unprotected drugs can be degraded before they are released at their intended target site.[10] To address premature degradation of drugs, several strategies can be employed including encapsulation of drugs into nano/microparticles, attaching drug-laden particles to the surface of macrophages, or manipulating phagosome maturation.[2,4,7,10,18−29] We have indeed previously successfully manipulated macrophages to ingest different cargoes—ranging from polystyrene particles to muscle stem cells—without the

Received: December 30, 2023
Revised: March 21, 2024
Accepted: April 1, 2024
Published: April 11, 2024

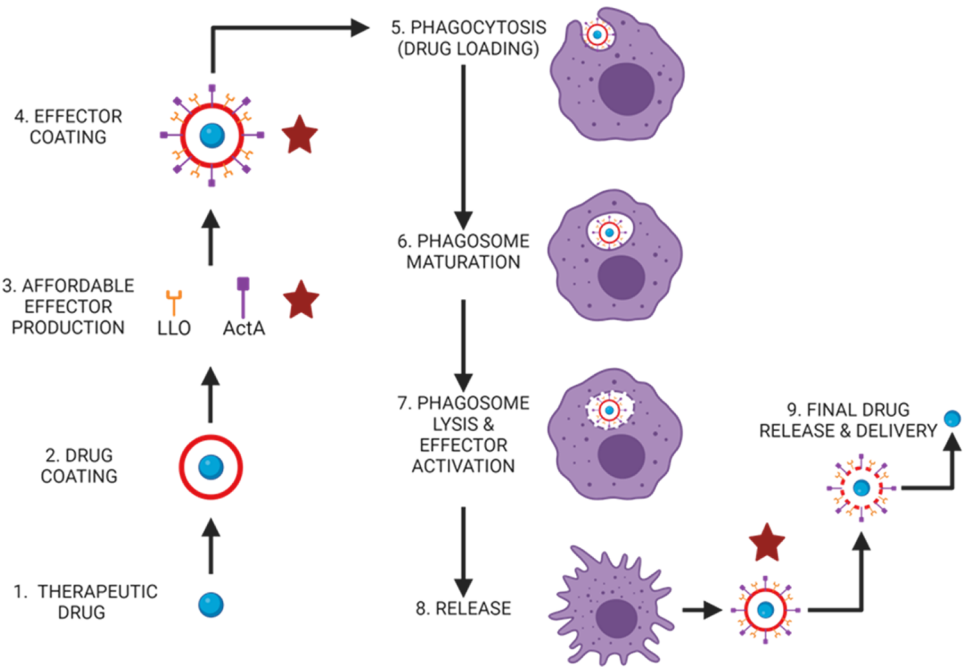

Figure 1. Deployment of a macrophage-based delivery system.

cargo being digested, by experimentally inducing transient phagosome maturation arrest in the macrophages.[10] Furthermore, we have shown sustained phagocytic and transendothelial migration capacity of these manipulated, loaded macrophages using *in vitro* cellular migration models.[10]

Second, phagocytosed drugs may be sequestered in phagosomes, which may result in inefficient drug release.[18] Thus, employment of a controllable, active drug release mechanism would allow the option for the timed release of drugs. To the best of our knowledge, such a mechanism does not yet exist. Most of the current methods rely on nonspecific release mechanisms, such as passive diffusion or methods that require carrier-cell death for release.[19,20,25,27,30,31] Previously, tunneling nanotubes have been described for the cell-to-cell delivery of doxorubicin (Dox) from M1 macrophages to tumor cells but was still associated with Dox leakage and reduced cell viability.[31] Methods to control the release of encapsulated drugs to delay their escape from macrophages include, among others, light-/temperature-sensitive polymeric formulations as well as pH-responsive and silica-based particles.[20,24,25,29,32] These methods, however, still rely on largely nonspecific mechanisms for the release of drugs/particles from the carrier cells.

Recently, we hypothesized that microbial effectors could be harnessed to achieve cargo release from carrier macrophages via known release mechanisms, which lends itself to better control over drug release.[33] Specifically, we hypothesized "hijacking" the mechanisms used by microbes (via specific microbial effectors) to induce their nonlytic release from cells during infection and *in vivo* dissemination[33] to produce a "synthetic microbe". In this approach, encapsulation of cargo with specific microbial effectors, prior to phagocytic loading into carrier macrophages, could then lead to their activation inside a macrophage phagosome to facilitate drug expulsion (Figure 1). Here, we describe the second phase of development of our proposed system, particularly focusing on the selection and synthesis of microbial effectors, as well as their efficacy in achieving drug release from carrier macrophages. In terms of the choice of microbial effectors, an important hallmark for effector identification is the nonlytic release of cargo from carrier cells. The majority of the literature describes a requirement for phagocytic engulfment with phagosomal manipulation by the microbe to maintain its own viability and even assist in its proliferation.[33,34] This immune evasion technique is then commonly followed by an actin polymerization-dependent mechanism of egress from the host cell. The mechanisms employed by *Listeria monocytogenes* was of particular interest in this context. The main effectors responsible for *L. monocytogenes* egress are listeriolysin-O (LLO) and actin assembly-inducing protein (ActA; see ref 35 for comprehensive review). The main function of LLO is to create pores in the phagosomal membrane when under acidic pH conditions, inducing bacterial escape into the cytosol.[36] Once in the cytosol, the activity of ActA is reported to induce actin polymerization in the more physiological pH of the cytosol.[37] These properties make LLO and ActA ideal candidate effectors for use in a drug delivery system based on endogenous phagocytic cells. They were thus selected as microbial effectors in the current study.

Given the extremely high cost of purified microbial effectors, and in particular that of LLO, we therefore first aimed to develop a cost-effective method for high-yield synthesis of these effectors to increase feasibility of this drug delivery system. Second, we evaluated the capacity of these effectors, when coated to simulated drug cargo, to facilitate cargo release from the carrier macrophages in a nonlytic manner, so that these macrophages may remain available on site to contribute to the resolution of inflammation.

The process begins with the core therapeutic drug that will be encapsulated for delivery (**1**). The drug is then encapsulated and coated for protection and controlled release (**2**). Microbial effector molecules such as LLO (listeriolysin-O) and ActA are heterologously produced to facilitate the controlled release of coated therapeutic (**3***). The encapsulated therapeutic is

https://doi.org/10.1021/acsomega.3c10519
ACS Omega 2024, 9, 18260−18272

coated with effectors (4*) to prepare for phagocytosis by macrophages (5). The phagosome within the macrophage matures, creating an environment for effector activation (6). Once activated, the effectors disrupt the phagosomal membrane (7), enabling the release of the coated therapeutic (8*). Once released at the target site, the outer protective layer around the therapeutic is dissembled and the therapeutic is released, completing the targeted delivery process (9). Areas focused on in the current study are indicated by stars. Figure created using BioRender.

MATERIALS AND METHODS

Materials, manufacturers, constructed plasmids, and buffer compositions (Tables S1 and S2) are described in the Supporting Information.

Below, we describe a novel homologous expression system for the high-yield synthesis of microbial effectors ActA and LLO.

Plasmid Design. The *L. monocytogenes* effectors LLO and ActA were translationally fused to green fluorescent protein (GFP) and expressed in *Escherichia coli*. Generation of a backbone plasmid containing *mgfp5* including an N-terminal 6× polyhistidine-tag (His tag) and C-terminal WELQut protease site was done according to previous reports (Figure S1).[38] Briefly, the *mgfp5* gene was amplified from pTRKH3-ermGFP using the primers listed in Table S2 and purified using the pJET PCR purification kit. The PCR product and pRSFDuet-1 were digested with the restriction enzymes *Bam*HI/*Pst*I. The digestion products were electrophoretically separated on an agarose gel, and bands were excised and purified from the gel pieces using the ZymoClean gel DNA recovery kit. Digestion products were ligated using T4 ligase, and the resulting pRSFGFP was used to transform chemically competent *E. coli* BL21 (DE3) cells. Transformants were plated onto Luria−Bertani (LB) agar supplemented with 50 μg/mL of kanamycin. Positive transformants were selected, and plasmid DNA was isolated using Pure Yield plasmid isolation kit. The *LLO* gene was amplified from *L. monocytogenes* EDG-e genomic DNA using the primers listed in Table S2, with the forward primer designed to exclude the N-terminal signal peptide. Digested (*Pst*I/NotI) and purified LLO was cloned into pRSFGFP on a *Pst*I/NotI fragment using T4 ligase, resulting in the translational fusion of LLO to His-tagged GFP (Figure S1a). The resulting pRSFGFP-LLO construct was transformed into chemically competent *E. coli* BL21 (DE3) cells.

Several plasmid constructs were generated for the expression of ActA (refer to the Supporting Information) due to degradation products observed during the expression and purification of ActA. The final construct resulted in the translational fusion of ActA to His-tagged GFP on its N-terminus and a GST tag on the C-terminus (Figure S1b). ActA was amplified from *L. monocytogenes* EDG-e gDNA with the primers designed to exclude the N- and C-terminal signal peptide and transmembrane domain, respectively (Figure S1b and Table S2). The GST tag was amplified from pET41a(+) using the primers listed in Table S2. The purified ActA PCR product was digested with *Pst*I/NotI and ligated into pRSFGFP previously digested with *Pst*I/NotI. The ligation product was transformed and purified. The resulting pRSFGFP-ActA construct was digested with NotI/XhoI and used in a ligation reaction with the GST tag (digested with NotI/XhoI). The product from the ligation reaction was used to transform chemically competent *E. coli* BL21 (DE3) cells and pDNA isolated as described previously. Stability of ActA during expression was increased using an *E. coli* strain, ArcticExpress, harboring the cold-adapted chaperonins Cpn10 and Cpn60. Transformation and culturing of ArcticExpress were performed as described for *E. coli* BL21 (DE3) except for gentamicin (20 μg/mL) being included to maintain the plasmid harboring *cpn10* and *cpn60*.

Protein Synthesis and Purification. *Listeriolysin-O.* *E. coli* expressing GFP-LLO was inoculated in LB broth containing 50 μg/mL of kanamycin and incubated overnight at 37 °C under agitation. For thio-B-D-galactopyranoside (IPTG) optimization, overnight cultures were used to inoculate 200 mL of Terrific Broth (TB; 1% v/v) containing 50 μg/mL of kanamycin. Flasks were incubated at 30 °C while shaking until an optical density ($OD_{600\ nm}$) of 0.6. Cells were induced with 0.25, 0.5, and 1.0 mM IPTG and expressed for 24 h at 26 °C with agitation. Cells were collected via centrifugation at 6164*g* for 20 min at 10 °C. The pellets were frozen before cells were lysed with 5 mL/g of lysis buffer (Table S1) for 30 min on ice. Cells were sonicated on ice at a 70% power output (90% pulses for 3 min) and centrifuged at 15,870*g* for 45 min at 10 °C. Prior to IMAC isolation, His Trap HP Ni-NTA His tag columns (1 mL) were equilibrated with SB30 followed by application of the cell-free supernatants. Columns were washed with SB30, and GFP-LLO was eluted using SB containing 500 mM of imidazole. The eluent was desalted against PBS (pH 7.4) using 10 kDa spin columns. Protein concentrations for yield determination of desalted proteins were determined using the BCA protein assay.

GFP-LLO concentration was adjusted to 1 mg/mL for the determination of optimal WELQut protease cleavage conditions. LLO was liberated from its GFP fusion partner by cleavage with 0.5 1.0, 5.0, and 10 U WELQut protease for 16 h at 26 °C in a total reaction volume of 25 μL. The optimal WELQut concentration was evaluated by sodium dodecyl sulphate-polyacrylamide gel electrophoresis (SDS-PAGE) analysis. Using optimal cleavage conditions, LLO was further purified to remove GFP and WELQut (also His-tagged). Imidazole was added at 10 mM and applied to an equilibrated His Trap HP Ni-NTA column. LLO containing flowthrough was collected, and the purified LLO was desalted with PBS (pH 7.4) using 10 kDa protein concentrators.

Actin Assembly-Inducing Protein. Purification of GFP-ActA-GST was done in a manner similar to that of GFP-LLO except for an additional GST-tag purification step (Figure S2). *E. coli* ArcticExpress cells expressing GFP-ActA-GST were inoculated in LB broth containing 50 μg/mL of kanamycin and 20 μg/mL of gentamycin and incubated overnight at 30 °C under agitation. This was inoculated in 500 mL of TB (2% v/v) containing 50 μg/mL of kanamycin and 20 μg/mL of gentamycin. Flasks were incubated at 30 °C while shaking until an $OD_{600\ nm}$ of 0.5 was reached. Cells were induced with 0.5 mM IPTG and allowed to express at 26 °C with agitation for 18 h. Cells were collected via centrifugation at 6164*g* for 20 min at 10 °C and lysed as described previously. All subsequent purification steps were done on ice to reduce the degradation of GFP-ActA-GST. Prior to protein isolation via IMAC, His Trap HP Ni-NTA His tag columns were equilibrated with SB containing 20 mM imidazole (SB20) supplemented with protease inhibitors, followed by the application of supernatant. Columns were washed twice, first with SB20 containing protease inhibitors followed by phosphate-buffered saline

https://doi.org/10.1021/acsomega.3c10519
ACS Omega 2024, 9, 18260−18272

(PBS) containing 20 mM imidazole (PBS20) before eluting GFP-ActA-GST with PBS containing 125 mM imidazole. The eluent was diluted 1:1 in PBS (pH 7.4) and supplemented with dithiothreitol (DTT) at a final concentration of 5 mM. The diluted eluent was applied to a column packed with glutathione agarose (2 mL) and circulated for 1 h to allow adequate binding of GST-tagged protein. Columns were washed with PBS (pH 7.4), and the bound GFP-ActA-GST eluted with PBS containing 10 mM reduced glutathione (pH 8).

Liberation of ActA-GST from GFP was achieved by WELQut cleavage. The GST-tag purification eluent was cleaved with 10 U WELQut protease per milliliter of eluent and incubated for 16 h at 8 °C. After cleavage, imidazole was added at 10 mM and applied to a His Trap HP Ni-NTA column pre-equilibrated with 10 mM imidazole. The liberated ActA-GST flowthrough was collected and desalted in 4-(2-hydroxyethyl)-1-piperazineethanesulfonic acid (HEPES) buffer (20 mM HEPES, 50 mM KCl; pH 7.5) using a 10 kDa protein concentrator, and protein yield was determined. Samples were collected through purification and cleavage reactions for analysis by SDS-PAGE.

SDS-PAGE. Samples were electrophoretically separated using tricine SDS-PAGE.[39] Briefly, samples were added to tricine sample buffer (1:1) and incubated at 37 °C for 30 min. Subsequently, 7 μL of sample was loaded into the wells of a 10% tricine SDS-PAGE gel. After separation, GFP fluorescence was visualized using either a MiniBIS Pro DNR Bioimaging system (DNR Bioimaging systems, Israel) or Dark Reader DR195 M Transilluminator (Integrated Scientific Solutions). Gels were fixed with 25% isopropanol and 10% acetic acid fixing buffer and stained using blue silver Coomassie stain (Table S1) until protein bands could be visualized.[40]

Preparation of Primary Human M1 Macrophages and Red Blood Cells. Ethical clearance exemption was obtained from the Subcommittee C Human Research Ethics Committee (HREC) of Stellenbosch University (ref no. X15/05/013) for isolation of primary human monocytes and erythrocytes from donor blood. Monocyte isolation, differentiation, and polarization into M1 macrophages were performed as previously described.[10]

Confirmation of Bioactivity of Synthesized LLO. Hemolytic activity (i.e., capacity for membrane perforation) of LLO and GFP-LLO was determined using human erythrocytes prepared from donated whole blood. GFP-LLO and LLO were made up to equal molar amounts (385 nM initial), which corresponded to 6500 ng/200 μL of GFP-LLO and 4300 ng/200 μL of LLO, respectively. Peripheral blood was centrifuged at 400*g* for 10 min, and plasma was removed. Erythrocytes were washed with PBS (pH 7.4) via centrifugation. The supernatant was removed, and erythrocytes were resuspended to the original volume followed by dilution at 1:50 in PBS at pH 7.4, 6.0, or 5.5 before 190 μL of these dilutions were mixed with 10 μL of LLO or GFP-LLO at varying concentrations. A positive control of 0.1% Triton X100 was included. Plates were incubated at 37 °C for 1 h before absorbance was measured at 540 nm. Zero (blank) and 100% hemolysis were determined using PBS (pH 7.4, 6.0, and 5.5) and 0.1% Triton X100, respectively. All other groups were expressed as a percentage of the positive control, as previously described.[41]

Microbial Effector Coating onto Simulated Drug Cargo. Effectors were coated onto 200 nm carboxylate-modified crimson polystyrene beads. Bead stock (3.4×10^{12} beads/mL) was diluted into 100 μL of 2-(*N*-morpholino) ethanesulfonic acid (MES) buffer (50 mM, pH 5.2) to a final concentration of 3.4×10^{11} beads/mL and incubated for 1 h at 23 °C. Beads were collected by centrifugation at 9400*g* for 10 min at 23 °C. The supernatant was removed, and LLO and ActA were added to beads at the final total protein concentrations of 47 and 45 μg, respectively, before incubation at 23 °C for 4 h. Beads were then washed three times with PBS before adding 100 μL of O+ donor serum. Effective bead coating was evaluated with SDS-PAGE and is discussed in the Supporting Information (Figure S3).

The actin polymerization activity of LLOActA- and ActA-coated beads was evaluated using isolated human macrophages and erythrocyte lysates, respectively. Human macrophages were isolated as previously described.[10] Isolated human macrophages (1×10^6 cells/mL) were treated with 3.4×10^8 cells/mL of serum beads or LLOActA beads and incubated at 37 °C with 5% CO_2 under 80% humidity 1 and 2 h, respectively, before being fixed with 4% paraformaldehyde for 10 min. Fixed cells were labeled with 1 μL/mL of Oregon Green Phalloidin and used for imaging. Actin polymerization activity of ActA-coated beads on erythrocyte lysates is discussed in the Supporting Information (Figure S4).

Evaluation of Potential Effector-Induced Cargo Bead Expulsion. Time-dependent expulsion of beads was assessed by exposing macrophage populations to either 6.8×10^8 LLOActA beads or serum-coated beads (Serum beads). Cells were incubated at 37 °C with 5% CO_2 under 80% humidity in separate 35 mm tissue culture dishes (Bio-Smart Scientific; 20035) for each time point. Culture dishes were removed from incubation from the 15 min time point at 5 min intervals up to 75 min; media was aspirated and replaced with 1 mL of 23 °C accutase (see the Supporting Information for additional details, Table S3). Dishes were incubated at 23 °C for 10 min before adding an additional 1 mL of 23 °C accutase and incubating for another 10 min. Cells were carefully scraped using a cell scraper and transferred to 15 mL tubes for centrifugation at 400*g* for 10 min at 23 °C. Pellets were resuspended in 200 μL of BD fixation/permeabilization solution containing 5 μL/mL of Hoechst and 0.25 μL/mL of Oregon Green Phalloidin. Suspensions were incubated at 4 °C for 20 min before centrifugation at 400*g* for 10 min at 23 °C. The stained cell pellet was resuspended in 50 μL of BD Perm/Wash solution before being analyzed on the ImageStream Mark II AMNIS imaging flow cytometer (Millipore Sigma, U.K.) using IDEAS acquisition software (version 6.2). Appropriate gates were drawn on the aspect ratio vs area graph to exclude debris, and the autosampler was set to record and count 10,000 events in the cell gate per sample (Figure S5). Illumination settings were set at 40 mW for 405 nm laser (Hoechst: nuclei), 100 mW for 488 nm (Oregon green phalloidin: actin), and 75 mW for the 642 nm laser (Crimson red: beads). Magnification was set at 60× with EDF (extended depth of field) selected and instrument set to the highest sensitivity with the lowest speed. A spot count analysis was set up to determine intracellular bead count. Cells were organized according to Intensity MC Channel11 (bead fluorescence channel). The low truth populations were chosen by selecting cells containing 0−1 bead, and high truth populations were chosen from cells containing the highest number of beads in this channel. A total of 50 cells were chosen for each truth population. To determine the average amount of beads/cell, the cumulative number of beads present in all bead-containing cells was

https://doi.org/10.1021/acsomega.3c10519
ACS Omega 2024, 9, 18260−18272

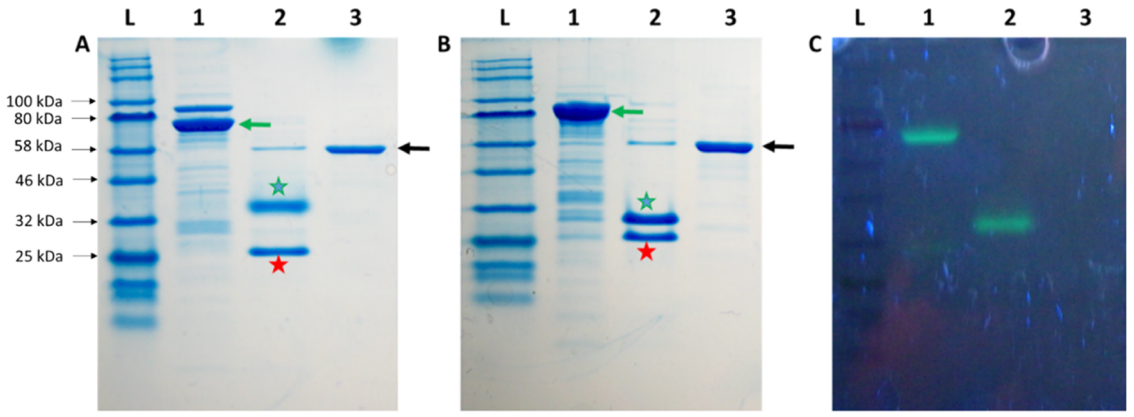

Figure 2. SDS-PAGE GFP-LLO and LLO treated at 37 °C (A) or 100 °C (B) before SDS-PAGE separation. Left: stained gel, right: fluorescent image of GFP-LLO (37 °C). L: ladder (NEB ladder #P7712), 1: GFP-LLO eluted from IMAC column, 2: GFP and WELQut eluted from the column after GFP-LLO digestion, 3: flowthrough from IMAC column containing LLO. GFP-LLO and LLO indicated with green and black arrows, respectively. GFP and WELQut protease indicated with green and red stars, respectively. (C) Fluorescent image of the gel depicted in the figure (A: boiling samples resulted in a loss of fluoresce).

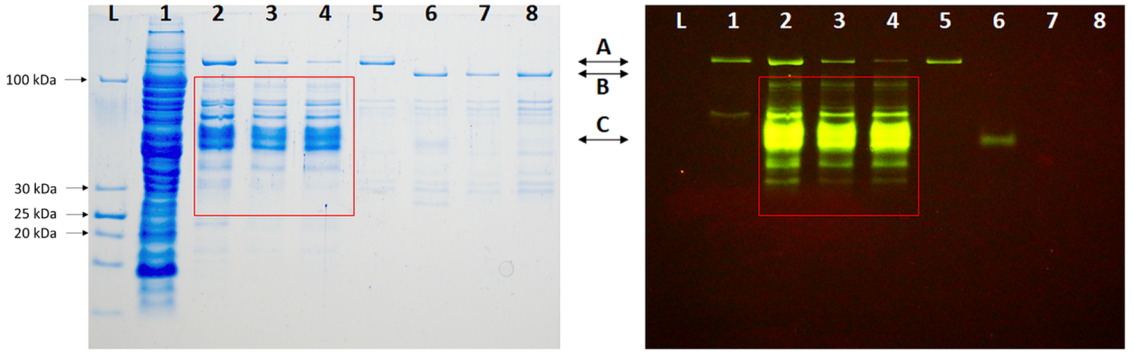

Figure 3. SDS-PAGE of GFP-ActA-GST purification. Left: stained gel, right: fluorescent images of GFP-ActA-GST and GFP in SDS-PAGE gel. L: ladder (PageRuler #26632), 1: IMAC flowthrough, 2: IMAC elution containing GFP-ActA-GST, 3: dilution of IMAC before GST purification, 4: flowthrough from GST column, 5: elution from a GST column containing GFP-ActA-GST, 6: WELQut protease cleavage of GFP-ActA-GST eluted from GST column, 7: flowthrough from the IMAC column containing ActA-GST after WELQut digestion, 8: desalted and concentrated ActA-GST obtained from IMAC flowthrough. A: GFP-ActA-GST, B: ActA-GST, C: GFP. Degradation products are outlined in red.

averaged according to the number of cells in the sample for each time point. To determine the number of cells that had undergone phagocytosis to take in beads, the percentage of cells containing one or more beads was recorded.

In addition to imaging flow cytometry, the more traditional technique of high-resolution microscopy was employed in parallel. Microscopy was conducted on a Carl Zeiss LSM780 confocal microscope with an ELYRA S.1 super-resolution platform (Carl Zeiss, Germany) and analyzed using ZEN black edition imaging software. Detailed methods of SR-SIM can be found in the Supporting Information.

Statistical Analysis. All statistical analysis was done using Graph Pad Prism 5. All data are presented as means ± SEM. Linear regression and analysis of variance (ANOVA, with Bonferroni post hoc tests) were conducted where appropriate. A p-value of <0.05 was considered statistically significant.

RESULTS

Heterologous Expression and Yield of LLO and ActA GFP Fusions. After the identification of the appropriate effectors to be evaluated in the synthetic microbe system, a suitable production system needed to be developed. To increase the solubility and stability of expressed effectors, we utilized GFP as a fusion partner.[38] Similar methods have also been employed for the expression of LLO[42] and ActA.[43] However, these studies did not focus on increasing protein yields, which is important if the system is to be translated into a viable therapeutic delivery system. Additionally, we utilized the fluorescent properties of GFP to monitor expression, purification, and downstream processes. This is a useful tool to quickly evaluate whether expression was successful, especially when trying to express bacterial toxins that may have deleterious effects on the expression host.

From SDS-PAGE analysis, fluorescent protein products corresponding to a size slightly lower than that of the expected size of GFP-LLO (~85 kDa), were observed (Figure 2). This can be explained by the fact that the samples were not boiled, as boiling would compromise GFP fluorescence, resulting in GFP-LLO migrating somewhat faster through the gel, thus visualizing at a smaller size equivalent when compared to the standard (Figure 2). Cleavage with WELQut was performed at several concentrations, and cleavage efficiency was evaluated using SDS-PAGE and fluorescent imaging. From SDS-PAGE analysis and corresponding fluorescent imaging, a clear drop in bands corresponding to LLO and GFP can be observed with increasing amounts of WELQut (Figure S6). Using a WELQut concentration of 0.4 U/μg resulted in the most effective removal of LLO from GFP and was used in subsequent larger-

https://doi.org/10.1021/acsomega.3c10519
ACS Omega 2024, 9, 18260−18272

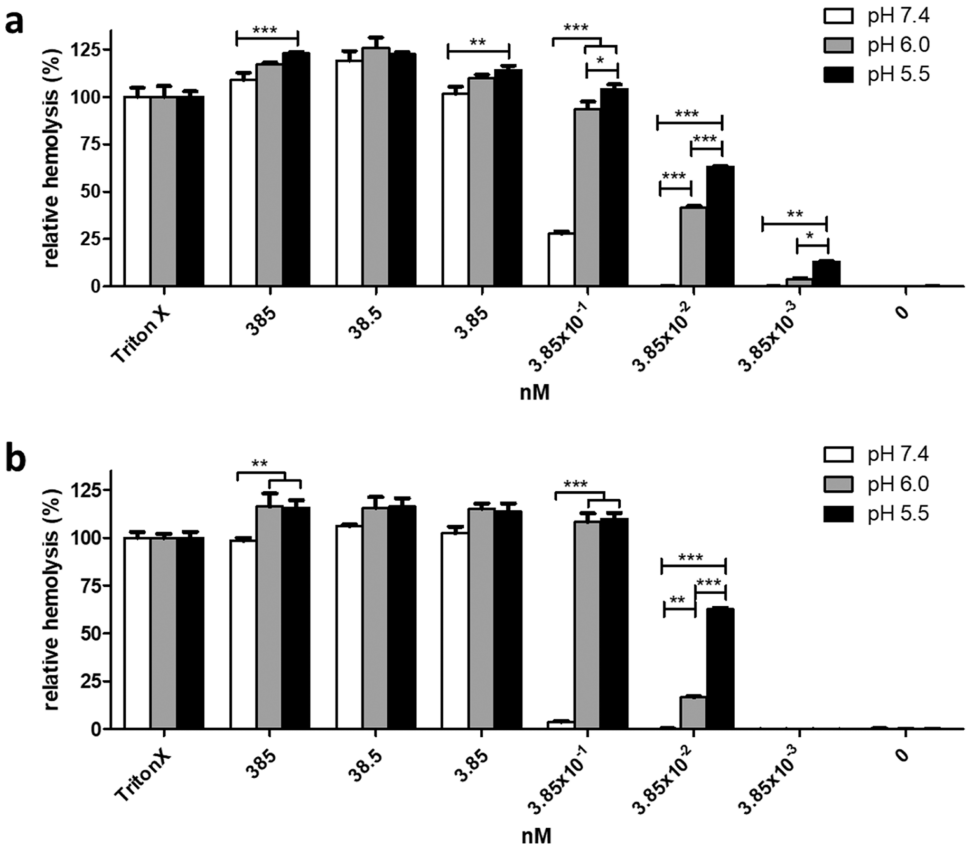

Figure 4. Erythrocyte hemolysis following LLO (a) and GFP-LLO (b) exposure at varying pH. Relative hemoglobin absorbance was collected at 540 nm; values are expressed as the percentage of positive control, mean ± SEM (n = 3). Analysis via two-way ANOVA where lines above bars indicate significance. *p < 0.05; **p < 0.01; ***p < 0.001.

scale cleavage reactions. Further separation of LLO from its fusion partner and from the protease was successfully achieved using His tag purification (Figure 2). Liberated LLO corresponded to the correct size with a single band corresponding to ∼56 kDa (Figures 1 and S6).

Optimal GFP-LLO yields were obtained when expression was induced with 0.5 mM IPTG, resulting in a GFP-LLO concentration of 109.01 mg/L and an LLO concentration (after cleavage and purification) of 51.48 mg/L.

Heterologous expression of ActA proved more difficult than that of LLO, with significant degradation observed in initial attempts (see the Supporting Information for details, Figure S7). To increase the yields of intact ActA, a dual purification method was used (Figure S2). His-tagged GFP and glutathione S-transferase (GST) were fused to the N- and C-terminals of ActA, respectively. Clear degradation was observed in samples collected from the first immobilized metal affinity chromatography (IMAC) purification steps (in red frames, Figure 3). The second purification step, utilizing the GST tag (and glutathione agarose), yielded the pure product with little to no degradation (lane 5 of Figure 3). It should be noted that ActA has previously been shown to have aberrant migration when separating with SDS-PAGE; this was ascribed to its high proline content.[43] After the cleavage of GFP-ActA-GST, a clear drop in the band (and fluorescence) corresponding to GFP could be observed along with the liberation of ActA-GST (lane 6 of Figure 3). Additional bands were observed after desalting and concentrating steps and may indicate a small degree of degradation of the ActA product during the 16 h cleavage step (lane 8 of Figure 3). The purity of ActA-GST, despite the observed evidence suggestive of some degradation, was deemed satisfactory for our purposes based on the retention of polymerization activity (Figures 5 and S4). Degradation of GFP-ActA-GST during expression and purification resulted in a lower yield when compared to that of GFP-LLO/LLO, with a final yield of ActA-GST of ∼890.35 μg/L (total protein).

Microbial Effector Activity Confirmed. The ability of LLO to form pores within membrane structures is well documented and may also be demonstrated by its ability to rupture erythrocyte membranes.[44,45] Thus, the activity of purified GFP-LLO and LLO was determined in terms of its capacity for hemolysis of human donor erythrocytes (sample purity represented in Figure 2). Previous reports have confirmed maintained activity of LLO following attachment to polystyrene beads.[46] Thus, we did not deem it necessary to incorporate a bead component in this validation step. Potent LLO hemolytic activity was observed at pH 6.0 and 5.5, with LLO concentrations as low as 3.85×10^{-3} nM resulting in some hemolysis (pH 6.0: 4.03 ± 0.45% and pH 5.5: 13.03 ± 0.46%), whereas significant reductions in hemolysis are observed at higher pH (no relative hemolysis at pH 7.4; Figure 4a). This trend is also seen at 3.85×10^{-2} nM LLO where a pH of 7.4 resulted in significantly less hemolysis (0.21 ± 0.06%) when compared to pH 6.0 and 5.5 (pH 6.0: 41.63 ± 0.84% and pH 5.5: 63.01 ± 0.65%). Thus, the purified LLO had potent activity by inducing hemolysis, especially at pH levels below that of physiological pH 7.4. Higher concentrations seemed to have saturated the sample to overcome pH dependency, subsequently inducing complete hemolysis at all pH levels including pH 7.4. Of note, an upward trend in

https://doi.org/10.1021/acsomega.3c10519
ACS Omega 2024, 9, 18260−18272

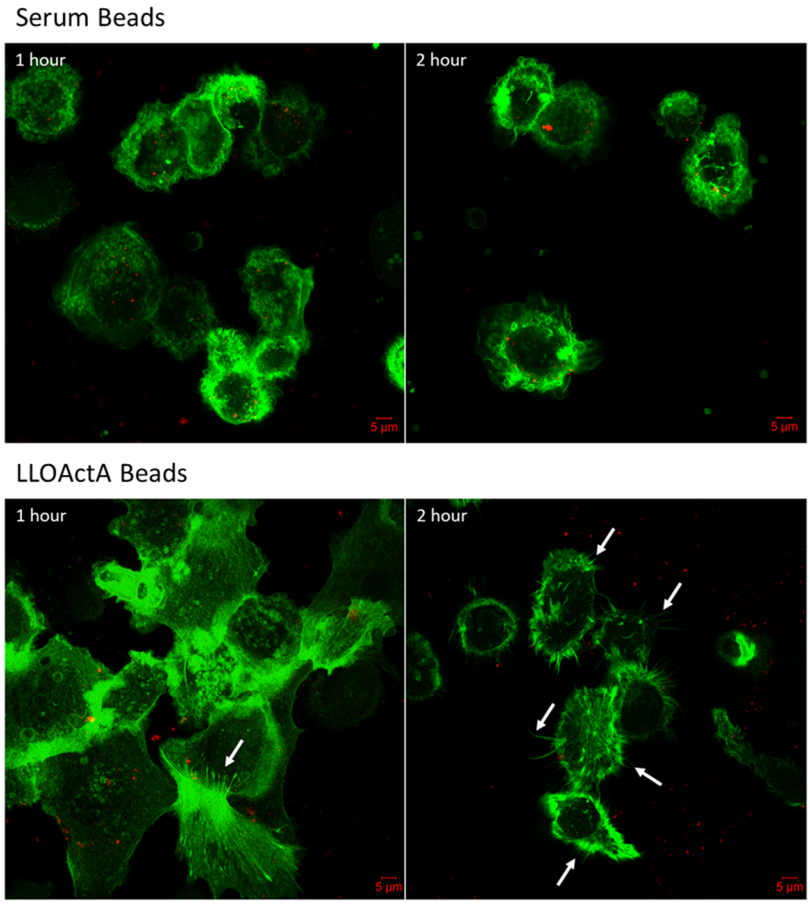

Figure 5. Confocal microscope assessment of actin polymerization. Images of separate cell populations exposed to serum beads and LLOActA beads, indicating the extent of actin polymerization (white arrows) at two time points.

hemolysis from pH 7.4 to 5.5 was still observed, indicating that pH levels may still play some role at higher concentrations. The hemolytic activity of GFP-LLO was similar to that of unfused LLO with activity below physiological pH at concentrations up to 3.85×10^{-2} nM (pH 6.0: 16.65 ± 0.78%, pH 5.5: 62.57 ± 1.32%; Figure 4b). Almost complete loss of hemolytic activity was observed at pH 7.4, at GFP-LLO concentrations of 3.85×10^{-1} nM (3.77 ± 0.513%), while the activity at pH 6.0 and 5.5 was still above 100%.

Bead Coating and Characterization of ActA Actin Polymerization Activity. The approximate concentration of the LLO and ActA-GST (intact) coating was determined at ∼21.02 and ∼11.09 μg, respectively, coated onto 3.4×10^{10} beads (Figure S3). From this, the calculated approximate bead loading efficiency for LLO onto the beads was 44.72% and for ActA (intact), 24.64%. From Figure S3, it was observed that all of the ActA bound to the beads, with some LLO still remaining in the supernatant. This may be due to the binding capacity of the beads being reached. Carboxylate-modified beads were used, as previous reports indicated that ActA does not bind to hydrophobic latex.[47] In addition, 0.22 μm beads were chosen due to previous reports of directional actin polymerization-induced movement following ActA coating of carboxylate-modified beads with a diameter of <0.5 μm.[48] Furthermore, current drug delivery systems utilize drug-containing particles of ∼0.2 μm in size, which corresponds to the size of our selected cargo-simulating beads.[49]

The activity of ActA was assessed in terms of its ability to polymerize actin by exposing erythrocyte lysates to polystyrene beads coated with ActA (ActA beads). Actin polymerization of actin from the erythrocyte membranes was observed in areas of bead localization (Figure S4).

Actin polymerization in the presence of beads coated with both LLO and ActA (LLOActA beads) was also confirmed *in vitro* using confocal microscopy (Figure 5, white arrows). After 2 h of exposure, human primary monocyte-derived macrophages exhibited greater actin polymerization and membrane extensions or "spikes" (white arrows) when compared to cells after 1 h. Additionally, these actin spikes were not observed in cells exposed to serum-coated beads (Figure 5). In hindsight, the data set would have been more complete with the addition of a group exposed to beads coated with ActA only. However, given the clear effect of the combination treatment, in our opinion, the omission of this group does not detract from the potential of using the bacterial effectors demonstrated here.

Potential for Cargo Expulsion: Quantitative Imaging Flow Cytometry and Qualitative High-Resolution Imaging Data. For initial evaluation, super-resolution structured illumination microscopy (SR-SIM) and confocal imaging were used to investigate bead uptake and localization (Figures S8 and S9). We were able to observe beads within cells for all treatments, with ActALLO-coated beads observed to be localized to the cell periphery (Figure S8). Phagocytosis was also observed, but due to the limited cell numbers per field of view (Figure S9), we opted to use a higher-throughput analytical tool for the generation of quantitative data, which aligns with the more modern practice of using flow cytometry to assess microbial manipulation of host cells.[50] Imaging flow

https://doi.org/10.1021/acsomega.3c10519
ACS Omega 2024, 9, 18260−18272

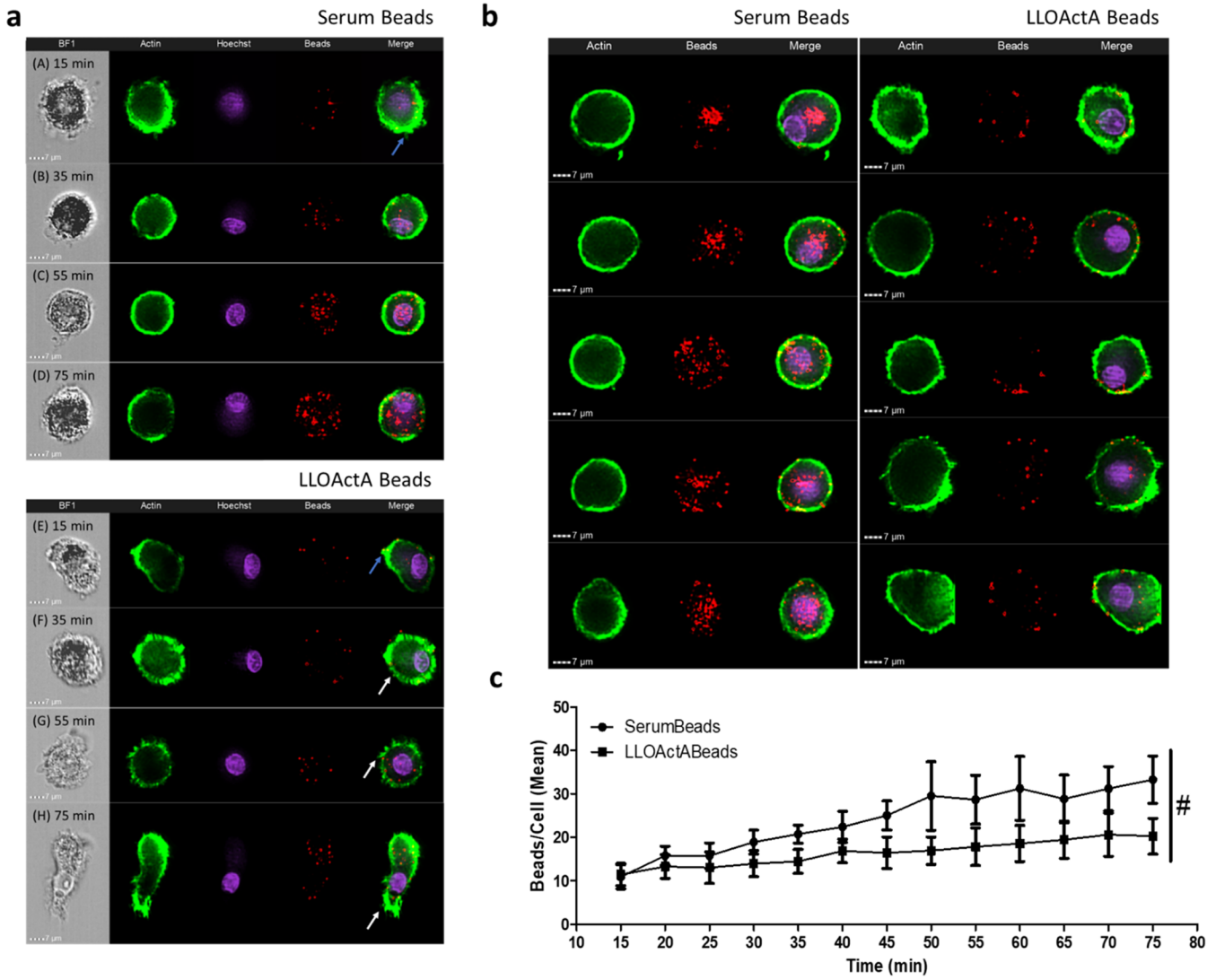

Figure 6. Phagocytic phases under control or effector-treated conditions over time. Macrophage populations were exposed to serum beads or LLOActA beads for different time periods and analyzed using imaging flow cytometry. (a) Accumulation of beads is seen under serum bead exposure. (b) Representative images of macrophages at 75 min suggest a tendency for bead distribution predominating at the periphery of cells during LLOActA bead exposure. (c) Number of beads per cell during exposure to serum beads and LLOActA beads. Average number of beads per cell given for effector-treated (LLOActA beads) and control (serum beads) over time. Blue arrows: pseudopodia; white arrows: actin membrane spikes; BF1: first bright-field channel. Data points are means, and error bars indicate SEM of 10,000 cells (n = 3 biological, 3 technical repeats per time point and condition). Statistics: #, ANOVA main effect of treatment, $p < 0.01$.

cytometry was chosen as a research tool for this purpose, as it generates data on thousands of cells (as opposed to typically <10 per field of view for confocal microscopy), thus removing bias and increasing detection sensitivity of the assessment technique. As we did not see any notable differences between beads coated with ActA and LLO using SR-SIM and confocal imaging, we only used serum and ActALLO-coated beads for imaging flow analysis. Images generated by imaging flow cytometry indicate morphological changes in cells undergoing different engulfment and what we interpret to be expulsion phases (Figure 6a). Initially, pseudopodia protrude from macrophages exposed to either serum beads or LLOActA beads at the 15 min time point, indicating that engulfment is initiated in similar time frames at this early time point when the effectors had not yet been activated (rows A and E of Figure 6a). Over time, gradual accumulation of beads inside macrophages was observed in cells exposed to serum beads but not those exposed to LLOActA beads (rows A–D and rows E–H of Figure 6b; ANOVA main effect of treatment, $p < 0.01$; Figure 6c), although the percentage of cells containing beads remained similar between the two groups over time (Figure S10). We interpreted these data as suggestive of the fact that the LLOActA combination had facilitated bead expulsion, thus preventing intracellular accumulation of these beads. Indeed, in line with effector activity assessments, almost all cells produced membrane spikes when exposed to LLOActA beads (rows F–H of Figure 6a). Of interest, when considering the location of intracellular beads, serum beads seemed to be homogeneously distributed throughout cells, whereas LLOActA beads were localized more toward the cell periphery (Figures 6b and S8). This is similar to what is observed in HeLa cells infected with *L. monocytogenes*,[51] providing further evidence that our effectors were functioning properly and in the way intended.

We do acknowledge that the data on potential cell expulsion may be perceived as circumstantial evidence only since the actual expulsion process was not visualized in real time using

https://doi.org/10.1021/acsomega.3c10519
ACS Omega 2024, 9, 18260−18272

high-resolution microscopy. Such data are required before a firm conclusion on data interpretation in terms of cargo expulsion is possible. However, this limitation does not detract from our data showing *in vivo* functionality of synthesized ActA and LLO.

DISCUSSION

Most research focused on the host−microbe interaction to date has been aimed at prevention of microbial infection or dissemination by identifying the active effectors or characterizing the redundant signaling pathways involved.[52,53] In contrast, here we set out to investigate whether microbial effectors could be used for therapeutic outcome. This builds on our previous work where ingestion and intracellular preservation of cargo by human macrophages were achieved while maintaining transmembrane migratory capacity of carrier cells.[10] Data presented here resulted from the reuse of this knowledge of microbes in a novel manner to engineer a system that would promote dissemination of beneficial components/compounds rather than microbes themselves. We present two sets of novel data. The first illustrates a novel methodology for the synthesis of microbial effectors to be used in the delivery system, while the second provides a proof-of-concept of the efficacy of these synthesized effectors to facilitate drug cargo expulsion from carrier macrophages.

In terms of effector synthesis, using a fusion-based system, we were able to heterologously express bioactive LLO and ActA in *E. coli*. Of specific interest was the heterologously expressed GFP-LLO. Previously, LLO has been purified from *L. monocytogenes* directly; however, these methods resulted in low yield and were relatively time-consuming.[44] These problems were overcome in the current study with the use of an *E. coli*-based expression system, which significantly increased yields while lowering production time. Of note, the heterologous GFP-linked LLO expression method resulted in significantly greater yields (51.48 mg/L) when compared to previously reported yields of 3.5−8 mg/L of LLO produced in *E. coli*.[45]

Methods for purification of ActA have also been established.[37,43,54,55] Using our heterologous expression and dual purification method, we isolated sufficient protein for experimentation to assess the feasibility of our proposed synthetic microbe system. The use of a dual-tagged (an N-terminal GST tag and a C-terminal His tag) system has previously been used for the expression of ActA.[43] Similar to the current results, attempts to remove the GST tag (with thrombin) resulted in multiple nonspecific bands. Interestingly, the N-terminal GST tag did not seem to significantly interfere with polymerization.[43] However, by removing the N-terminal GFP-tag, the resulting ActA-GST product more closely resembled that of native ActA as found on the membrane of *L. monocytogenes*, which may aid in proper motility of the synthetic microbe. Furthermore, using our heterologous expression method, we were able to visualize expression (through GFP fluorescence) as well as degradation during the different purification steps without the need for Western blots, thereby again saving both time and costs. It should be noted that both ActA and LLO yields can be further increased by optimizing production and lysis methods.

In terms of potential mechanisms by which these effectors may facilitate drug delivery via expulsion from carrier macrophages, although molecular motors have been discussed in the literature for potential use in drug/gene delivery, the use of ActA as a molecular motor has not been investigated.[56] However, since *L. monocytogenes* has been shown to use interactions with transmembrane proteins such as the adhesion molecule CD147 to form membrane protrusions for its dissemination,[57] and since actin network disruption (which is a function of ActA) has been linked to increased cell membrane permeability,[57] elucidation of the exact mechanism of action of ActA should be investigated within a therapeutic paradigm. LLO, on the other hand, has been investigated in the context of the delivery of macromolecules to the cytosol of cells[58−60] due to its well-documented ability to disrupt phagosomal membranes.[44,45] While neither of these effectors would be able to induce cellular expulsion mechanisms in its entirety, the combination of the two seems to be able to achieve a feasible synergistic effector system.

In terms of efficacy in terms of drug expulsion, the fact that macrophages exposed to LLOActA beads presented marked actin polymerization as well as clear membranous actin spikes is in accordance with reports of actin-propelled membrane protrusions that are taken up by adjacent cells during *L. monocytogenes* dissemination from cell to cell.[61] In this well-described process, the plasma membrane of protrusions formed from infected cells is damaged by LLO, resulting in surface presentation of the inner membrane leaflet lipid phosphatidylserine (PS). These PS+ protrusions are recognized by the T-cell immunoglobulin and mucin-domain-containing protein 4 (TIM-4) on macrophages, which subsequently mediates the uptake of PS+ protrusions.[62] Expelled bacteria may also be packed into PS+ vesicles formed because of Ca^{2+}-dependent membrane repair and scission of the initial PS+ protrusion.[62] We propose that our data may suggest the potential expulsion of cargo as PS+ vesicles, although this mechanism remains to be confirmed in a purpose-designed study. The gradual accumulation of serum-coated beads within macrophages, while LLOActA-coated beads did not, supports this interpretation. In addition, the localization of LLOActA-coated beads on the cellular periphery (while serum-coated beads did not) further argues for successful "escape" of cargo from phagosomes via LLO-mediated perforation and ActA-mediated modulation of membrane mechanics to induce membrane protrusion formation. The peripheral location of beads can be attributed to ActA's interaction with the host's actin cytoskeleton where actin polymerization directs beads toward the cell membrane. An alternative interpretation of the data indicating accumulation of serum-coated beads only may be greater uptake of serum- vs LLOActA-coated beads, instead of expulsion of LLOActA-coated beads. However, this is unlikely for three reasons: first, LLO is known to promote bacterial cell uptake,[46] so it is unlikely to negatively affect uptake; second, at all-time points during the protocol, an equal percentage of macrophages contains beads irrespective of coating (Figure S10), which again argues against limited uptake capacity; and third, the number of beads/cell (Figure 6c) is equal at 15 min—this time point is sufficiently late to have allowed for completed phagocytosis cycles but too early for phagosome acidification and effector activation (i.e., expulsion), which is typically reported to initiate between 15 and 30 min after engulfment and phagosome formation.[63] Thus, successful cargo expulsion remains a more likely interpretation. The next step would be to validate this in an *in vivo* system, such as larval zebrafish, whose natural transparency at larval stages allows for live imaging and

https://doi.org/10.1021/acsomega.3c10519
ACS Omega 2024, 9, 18260−18272

which has been shown to be compatible with injected human macrophages for at least up to 2 weeks.[64]

Looking forward, apart from *in vivo* validation of the complete system, additional optimization envisaged includes the combination of our current approach with advanced smart polymers to control the specific release of effectors as well as therapeutics. We have proposed the use of multilayered polymer formulations or multistage delivery systems for the controlled release of effectors and therapeutics.[33] For example, a combination of pH-sensitive polymer formulations and maturation arrest can be employed.[10,25,65] Previously, we have shown that phagosome acidification can be delayed by treating macrophages with a wortmannin−concanamycin A−chloroquine cocktail.[10] Maturation arrest alone or in combination with pH-sensitive polymeric particles would allow sufficient time for macrophage migration toward target areas before the release of effectors and initiation of drug release. Alternatively, the use of photosensitive formulations has been shown to be effective for the triggered release of therapeutics. Recently, Zhao et al. illustrated the use of a dual-wavelength photosensitive system where the release of drugs could be specifically controlled using near-infrared light (690 and 808 nm).[66] These methods could be employed to specifically trigger the release of effectors and drugs from multilayered formulations, and further investigations into these approaches are ongoing.

In summary, the heterologous expression systems developed optimized and presented here are effective in producing bioactive microbial effectors at high yield. Although the synthetic microbe prototype remains to be further optimized and tested using *in vivo* models, data presented here illustrates the significant potential of using microbial effectors for therapeutic benefit that would allow for the specific release of effectors and drugs at specific sites. Further research is required to optimize the formulations that can be used to fully unlock the potential of microbial effectors for effective drug delivery and release in cell-based delivery systems. However, this could initiate a paradigm shifting research area pertaining to the treatment of a plethora of diseases, which are currently hampered by limitations such as poor blood supply or high toxicity of pharmaceuticals.

■ ASSOCIATED CONTENT

Data Availability Statement

The data sets used and analyzed during the current study are available from the corresponding author on reasonable request to the corresponding author Prof Carine Smith.

Supporting Information

The Supporting Information is available free of charge at https://pubs.acs.org/doi/10.1021/acsomega.3c10519.

Additional experimental details, materials, and methods, including photographs of experimental setup; Figure S1 (a, b): plasmid maps and nucleotide/amino acid sequences of interest for pRSF_GFPLLO (construct containing GFP fused to LLO) and pRSF_GFPnoSSActA_GST (construct containing GFP and GST fused to ActA); Figure S2: schematic diagram illustrating the purification workflow for GFPActAGST; Figure S3: SDS-PAGE gel image used for analysis to determine the amount of LLO and ActA before and after coating onto beads; Figure S4: fluorescent confocal images illustrating actin polymerization in erythrocyte after exposure to ActA- or serum-coated beads; Figure S5 (a−h): graphs from a coated bead sample analysis obtained from imaging flow cytometry: (1) histogram showing all events at various time points of coated bead samples according to gradient RMS values obtained through widefield microscopy. (2) Scatter plot of "focused" population at various time points of coated bead samples according to area vs aspect ratio obtained through widefield microscopy. (3) Bar graphs of "singlets" population at various time points of coated bead samples according to the number cells (normalized frequency) over the number of beads counted within the cells (spot count); Figure S6: SDS-PAGE image illustrating the cleavage efficiency of GFP-LLO using WELQut protease; Figure S7: SDS-PAGE image illustrating ActA degradation; Figure S8: SR-SIM images of macrophages exposed to beads coated with serum, ActA, LLO, or ActALLO at 75 and 120 min; Figure S9: SR-SIM images of macrophages to illustrate the extension of pseudopodia toward coated beads; Figure S10: graph illustrating the percentage of cells actively participating in phagocytosis when exposed to serum beads or LLOActA beads; Table S1: buffers/media and their formulation used for the expression and purification of microbial effectors; Table S2: primers and their respective sequences used for the cloning of microbial effectors; and Table S3: viable cell yield and membrane marker retention using different cell processing protocols (PDF)

■ AUTHOR INFORMATION

Corresponding Authors

Anton Du Preez Van Staden − *Department of Microbiology, Science Faculty, Stellenbosch University, Stellenbosch 7600, South Africa; Experimental Medicine Research Group, Department of Medicine, Faculty of Medicine and Health Sciences, Stellenbosch University, Parow 7505, South Africa;* orcid.org/0000-0003-0596-8849; Email: advstaden@sun.ac.za

Carine Smith − *Experimental Medicine Research Group, Department of Medicine, Faculty of Medicine and Health Sciences, Stellenbosch University, Parow 7505, South Africa;* orcid.org/0000-0001-5924-9204; Email: csmith@sun.ac.za

Authors

Johan G. Visser − *Department of Physiological Sciences, Science Faculty, Stellenbosch University, Stellenbosch 7602, South Africa;* orcid.org/0000-0002-4614-4494

Yigael S. L. Powrie − *Experimental Medicine Research Group, Department of Medicine, Faculty of Medicine and Health Sciences, Stellenbosch University, Parow 7505, South Africa; Division of Neurosurgery, University of Cape Twon, Cape Town 7925, South Africa*

Complete contact information is available at: https://pubs.acs.org/10.1021/acsomega.3c10519

Author Contributions

All authors: methodology, formal analysis, and writing—original draft preparation. A.D.P.V.S., J.G.V., and Y.S.L.P.: investigation. A.D.P.V.S. and C.S.: conceptualization, writing—review and editing, supervision of J.G.V.; C.S.: funding acquisition.

https://doi.org/10.1021/acsomega.3c10519
ACS Omega 2024, 9, 18260−18272

Funding

The authors thank the National Research Foundation of South Africa (grant no.: BS170501229280), the University of Stellenbosch and professors Robert Fenn and Jean Millar for financial assistance.

Notes

The authors declare no competing financial interest.

Ethics Approval Ethical clearance exemption was obtained from the Subcommittee C Human Research Ethics Committee (HREC) of Stellenbosch University (Reference #X15/05/013) for isolation of primary human monocytes and erythrocytes from donor blood. Recruitment of human donors was managed through the Western Cape Blood Transfusion Service. Donors from their database were contacted and recruited on a voluntary basis. All donors completed a project-specific consent form.

Consent for Publication All authors agreed to the final version of this manuscript.

■ ACKNOWLEDGMENTS

Lize Engelbrecht and Dr. Dalene de Swart are acknowledged for technical assistance with fluorescence microscopy and flow cytometry and Prof. James Lloyd (Stellenbosch University) and Dr. Michela Lizier (Addgene) for providing plasmids.

■ REFERENCES

(1) Liang, T.; Zhang, R.; Liu, X.; Ding, Q.; Wu, S.; Li, C.; Lin, Y.; Ye, Y.; Zhong, Z.; Zhou, M. Recent Advances in Macrophage-Mediated Drug Delivery Systems. *Int. J. Nanomed.* **2021**, *16*, 2703−2714, DOI: 10.2147/IJN.S298159.

(2) Hou, T.; Wang, T.; Mu, W.; Yang, R.; Liang, S.; Zhang, Z.; Fu, S.; Gao, T.; Liu, Y.; Zhang, N. Nanoparticle-Loaded Polarized-Macrophages for Enhanced Tumor Targeting and Cell-Chemo-therapy. *Nano-Micro Lett.* **2021**, *13*, No. 6, DOI: 10.1007/s40820-020-00531-0.

(3) Wang, H.-F.; Liu, Y.; Yang, G.; Zhao, C.-X. Macrophage-mediated cancer drug delivery. *Mater. Today Sustainability* **2020**, *11*, No. 100055, DOI: 10.1016/j.mtsust.2020.100055.

(4) Tanei, T.; Leonard, F.; Liu, X.; Alexander, J. F.; Saito, Y.; Ferrari, M.; Godin, B.; Yokoi, K. Redirecting Transport of Nanoparticle Albumin-Bound Paclitaxel to Macrophages Enhances Therapeutic Efficacy against Liver Metastases. *Cancer Res.* **2016**, *76*, 429−439, DOI: 10.1158/0008-5472.CAN-15-1576.

(5) Qin, Y.; Wang, Y.; He, Y.; Zhang, Y.; She, Q.; Chai, Y.; Li, P.; Shang, Q. Characterization of Subtilin L-Q11, a Novel Class I Bacteriocin Synthesized by Bacillus subtilis L-Q11 Isolated From Orchard Soil. *Front. Microbiol.* **2019**, *10*, No. 484, DOI: 10.3389/fmicb.2019.00484.

(6) Xuan, M.; Shao, J.; Dai, L.; He, Q.; Li, J. Macrophage Cell Membrane Camouflaged Mesoporous Silica Nanocapsules for In Vivo Cancer Therapy. *Adv. Healthcare Mater.* **2015**, *4*, 1645−1652.

(7) Miller, M. A.; Zheng, Y.-R.; Gadde, S.; Pfirschke, C.; Zope, H.; Engblom, C.; Kohler, R. H.; et al. Tumour-associated macrophages act as a slow-release reservoir of nano-therapeutic Pt(IV) pro-drug. *Nat. Commun.* **2015**, *6*, No. 8692.

(8) Li, R.; He, Y.; Zhu, Y.; Jiang, L.; Zhang, S.; Qin, J.; Wu, Q.; et al. Route to Rheumatoid Arthritis by Macrophage-Derived Microvesicle-Coated Nanoparticles. *Nano Lett.* **2019**, *19*, 124−134.

(9) Kruger, M. J.; Myburgh, K. H.; Smith, C. Contusion injury with chronic in vivo polyphenol supplementation: leukocyte responses. *Med. Sci. Sports Exercise* **2014**, *46*, 225−231.

(10) Visser, J. G.; Smith, C. Development of a transendothelial shuttle by macrophage modification. *J. Tissue Eng. Regener. Med.* **2018**, *12*, e1889−e1898.

(11) Wynn, T. A.; Chawla, A.; Pollard, J. W. Macrophage biology in development, homeostasis and disease. *Nature* **2013**, *496*, 445−455.

(12) Tacke, F. Targeting hepatic macrophages to treat liver diseases. *J. Hepatol.* **2017**, *66*, 1300−1312.

(13) Shapouri-Moghaddam, A.; Mohammadian, S.; Vazini, H.; Taghadosi, M.; Esmaeili, S.-A.; Mardani, F.; Seifi, B.; Mohammadi, A.; Afshari, J. T.; Sahebkar, A. Macrophage plasticity, polarization, and function in health and disease. *J. Cell. Physiol.* **2018**, *233*, 6425−6440.

(14) Noy, R.; Pollard, J. W. Tumor-Associated Macrophages: From Mechanisms to Therapy. *Immunity* **2014**, *41*, 49−61.

(15) Guo, Q.; Jin, Z.; Yuan, Y.; Liu, R.; Xu, T.; Wei, H.; Xu, X.; et al. New Mechanisms of Tumor-Associated Macrophages on Promoting Tumor Progression: Recent Research Advances and Potential Targets for Tumor Immunotherapy. *J. Immunol. Res.* **2016**, *2016*, 1−12.

(16) Thamphiwatana, S.; Angsantikul, P.; Escajadillo, T.; Zhang, Q.; Olson, J.; Luk, B. T.; Zhang, S.; et al. Macrophage-like nanoparticles concurrently absorbing endotoxins and proinflammatory cytokines for sepsis management. *Proc. Natl. Acad. Sci. U.S.A.* **2017**, *114*, 11488−11493.

(17) Rayamajhi, S.; Nguyen, T. D. T.; Marasini, R.; Aryal, S. Macrophage-derived exosome-mimetic hybrid vesicles for tumor targeted drug delivery. *Acta Biomater.* **2019**, *94*, 482−494.

(18) Doshi, N.; Swiston, A. J.; Gilbert, J. B.; Alcaraz, M. L.; Cohen, R. E.; Rubner, M. F.; Mitragotri, S. Cell-Based Drug Delivery Devices Using Phagocytosis-Resistant Backpacks. *Adv. Mater.* **2011**, *23*, H105−H109, DOI: 10.1002/adma.201004074.

(19) Choi, J.; Kim, H.-Y.; Ju, E. J.; Jung, J.; Park, J.; Chung, H.-K.; Lee, J. S.; et al. Use of macrophages to deliver therapeutic and imaging contrast agents to tumors. *Biomaterials* **2012**, *33*, 4195−4203, DOI: 10.1016/j.biomaterials.2012.02.022.

(20) Choi, M.-R.; Katie, J. S.-M.; Stanley, J. K.; Levin, C. S.; Bardhan, R.; Akin, D.; Badve, S.; et al. A Cellular Trojan Horse for Delivery of Therapeutic Nanoparticles into Tumors. *Nano Lett.* **2007**, *7*, 3759−3765.

(21) Chang, Y.-N.; Guo, H.; Li, J.; Song, Y.; Zhang, M.; Jin, J.; Xing, G.; Zhao, Y. Adjusting the Balance between Effective Loading and Vector Migration of Macrophage Vehicles to Deliver Nanoparticles. Edited by Gianfranco Pintus. *PLoS One* **2013**, *8*, No. e76024, DOI: 10.1371/journal.pone.0076024.

(22) Blaudszun, A.-R.; Lian, Q.; Schnabel, M.; Loretz, B.; Steinfeld, U.; Lee, H.-H.; Wenz, G.; Lehr, C.-M.; Schneider, M.; Philippi, A. Polyester-idarubicin nanoparticles and a polymer-photosensitizer complex as potential drug formulations for cell-mediated drug delivery. *Int. J. Pharm.* **2014**, *474*, 70−79, DOI: 10.1016/j.ijpharm.2014.07.048.

(23) Batrakova, E. V.; Li, S.; Reynolds, A. D.; Mosley, R. L.; Bronich, T. K.; Kabanov, A. V.; Gendelman, H. E. A Macrophage−Nanozyme Delivery System for Parkinson's Disease. *Bioconjugate Chem.* **2007**, *18*, 1498−1506, DOI: 10.1021/bc700184b.

(24) Evans, M. A.; Huang, P.-J.; Iwamoto, Y.; Ibsen, K. N.; Chan, E. M.; Hitomi, Y.; Ford, P. C.; Mitragotri, S. Macrophage-mediated delivery of light activated nitric oxide prodrugs with spatial, temporal and concentration control. *Chem. Sci.* **2018**, *9*, 3729−3741, DOI: 10.1039/C8SC00015H.

(25) Lang, T.; Dong, X.; Huang, Y.; Ran, W.; Yin, Q.; Zhang, P.; Zhang, Z.; Yu, H.; Li, Y. Ly6C hi Monocytes Delivering pH-Sensitive Micelle Loading Paclitaxel Improve Targeting Therapy of Metastatic Breast Cancer. *Adv. Funct. Mater.* **2017**, *27*, No. 1701093, DOI: 10.1002/adfm.201701093.

(26) Zhao, Y.; Haney, M. J. Active Targeted Macrophage-mediated Delivery of Catalase to Affected Brain Regions in Models of Parkinson's Disease. *J. Nanomed. Nanotechnol.* **2011**, *01*, No. 003, DOI: 10.4172/2157-7439.S4-003.

(27) Pang, L.; Qin, J.; Han, L.; Zhao, W.; Liang, J.; Xie, Z.; Yang, P.; Wang, J. Exploiting macrophages as targeted carrier to guide nanoparticles into glioma. *Oncotarget* **2016**, *7*, 37081−37091, DOI: 10.18632/oncotarget.9464.

(28) Gnanadhas, D. P.; Dash, P. K.; Sillman, B.; Bade, A. N.; Lin, Z.; Palandri, D. L.; Gautam, N.; et al. Autophagy facilitates macrophage depots of sustained-release nanoformulated antiretroviral drugs. *J. Clin. Invest.* **2017**, *127*, 857−873, DOI: 10.1172/JCI90025.

(29) Ikehara, Y.; Niwa, T.; Biao, L.; Ikehara, S. K.; Ohashi, N.; Kobayashi, T.; Shimizu, Y.; Kojima, N.; Nakanishi, H. A Carbohydrate Recognition−Based Drug Delivery and Controlled Release System using Intraperitoneal Macrophages as a Cellular Vehicle. *Cancer Res.* **2006**, *66*, 8740−8748, DOI: 10.1158/0008-5472.CAN-06-0470.
(30) Fu, J.; Wang, D.; Mei, D.; Zhang, H.; Wang, Z.; He, B.; Dai, W.; Zhang, H.; Wang, X.; Zhang, Q. Macrophage mediated biomimetic delivery system for the treatment of lung metastasis of breast cancer. *J. Controlled Release* **2015**, *204*, 11−19, DOI: 10.1016/j.jconrel.2015.01.039.
(31) Guo, L.; Zhang, Y.; Yang, Z.; Peng, H.; Wei, R.; Wang, C.; Feng, M. Tunneling Nanotubular Expressways for Ultrafast and Accurate M1Macrophage Delivery of Anticancer Drugs to Metastatic Ovarian Carcinoma. *ACS Nano* **2019**, *13*, No. 8b08872, DOI: 10.1021/acsnano.8b08872.
(32) Zhang, W.; Wang, M.; Tang, W.; Wen, R.; Zhou, S.; Lee, C.; Wang, H.; et al. Nanoparticle-Laden Macrophages for Tumor-Tropic Drug Delivery. *Adv. Mater.* **2018**, *30*, No. 1805557.
(33) Visser, J. G.; Van Staden, A. D. P.; Smith, C. Harnessing Macrophages for Controlled-Release Drug Delivery: Lessons From Microbes. *Front. Pharmacol.* **2019**, *10*, 1−18.
(34) Martinez, E.; Siadous, F. A.; Bonazzi, M. Tiny architects: biogenesis of intracellular replicative niches by bacterial pathogens. *FEMS Microbiol. Rev.* **2018**, *42*, 425−447.
(35) Radoshevich, L.; Cossart, P. Listeria monocytogenes: towards a complete picture of its physiology and pathogenesis. *Nat. Rev. Microbiol.* **2018**, *16*, 32−46, DOI: 10.1038/nrmicro.2017.126.
(36) Alberti-Segui, C.; Goeden, K. R.; Higgins, D. E. Differential function of Listeria monocytogenes listeriolysin O and phospholipases C in vacuolar dissolution following cell-to-cell spread. *Cell. Microbiol.* **2007**, *9*, 179−195.
(37) Skoble, J.; Welch, M. D.; Skoble, J.; Portnoy, D. A.; Welch, M. D. Three regions within ActA promote Arp2/3 complex-mediated actin nucleation and listeria monocytogenes motility Three Regions within ActA Promote Arp2/3 Complex-mediated Actin Nucleation and Listeria monocytogenes Motility. *J. Cell. Biol.* **2000**, *150*, 527−537.
(38) Van Staden, A. D. P.; Faure, L. M.; Vermeulen, R. R.; Dicks, L. M. T.; Smith, C. Functional Expression of GFP-Fused Class I Lanthipeptides in *Escherichia coli*. *ACS Synth. Biol.* **2019**, *8*, 2220−2227.
(39) Schägger, H. Tricine−SDS-PAGE. *Nat. Protoc.* **2006**, *1*, 16−22, DOI: 10.1038/nprot.2006.4.
(40) Candiano, G.; Bruschi, M.; Musante, L.; Santucci, L.; Ghiggeri, G. M.; Carnemolla, B.; Orecchia, P.; Zardi, L.; Righetti, P. G. Blue silver: A very sensitive colloidal Coomassie G-250 staining for proteome analysis. *Electrophoresis* **2004**, *25*, 1327−1333, DOI: 10.1002/elps.200305844.
(41) van Staden, A. D.; Brand, A. M.; Dicks, L. M. T. Nisin F-loaded brushite bone cement prevented the growth of Staphylococcus aureus in vivo. *J. Appl. Microbiol.* **2012**, *112*, 831−840.
(42) Kwiatkowska, A.; Granicka, L. H.; Grzeczkowicz, A.; Stachowiak, R.; Kamiński, M.; Grubek, Z.; Bielecki, J.; Strawski, M.; Szklarczyk, M. Stabilized nanosystem of nanocarriers with an immobilized biological factor for anti-tumor therapy. Edited by Bing Xu. *PLoS One* **2017**, *12*, No. e0170925.
(43) Noireaux, V.; Golsteyn, R. M.; Friederich, E.; Prost, J.; Antony, C.; Louvard, D.; Sykes, C. Growing an Actin Gel on Spherical Surfaces. *Biophys. J.* **2000**, *78*, 1643−1654, DOI: 10.1016/S0006-3495(00)76716-6.
(44) Traub, W. H.; Bauer, D. Simplified purification of Listeria monocytogenes listeriolysin O and preliminary application in the enzyme-linked immunosorbent assay (ELISA). *Int. J. Med. Microbiol.* **1995**, *283*, 29−42.
(45) Churchill, R. L. T.; Lee, H.; Hall, J. C. Rapid purification of recombinant listeriolysin O (LLO) from *Escherichia coli*. *J. Ind. Microbiol. Biotechnol.* **2005**, *32*, 355−363.
(46) Vadia, S.; Arnett, E.; Haghighat, A.-C.; Wilson-Kubalek, E. M.; Tweten, R. K.; Seveau, S. The Pore-Forming Toxin Listeriolysin O Mediates a Novel Entry Pathway of L. monocytogenes into Human Hepatocytes. Edited by Guy Tran Van Nhieu. *PLoS Pathog.* **2011**, *7*, No. e1002356.
(47) Footer, M. J.; Lyo, J. K.; Theriot, J. A. Close Packing of Listeria monocytogenes ActA, a Natively Unfolded Protein, Enhances F-actin Assembly without Dimerization. *J. Biol. Chem.* **2008**, *283*, 23852−23862.
(48) Cameron, L. A.; Footer, M. J.; Oudenaarden, A. v.; Theriot, J. A. Motility of ActA protein-coated microspheres driven by actin polymerization. *Proc. Natl. Acad. Sci. U.S.A.* **1999**, *96*, 4908−4913.
(49) Kleynhans, J.; Elgar, D.; Ebenhan, T.; Zeevaart, J. R.; Kotzé, A.; Grobler, A. A toxicity profile of the Pheroid technology in rodents. *Toxicol. Rep.* **2019**, *6*, 940−950.
(50) Evans, R. J.; Voelz, K.; Johnston, S. A.; May, R. C. Using Flow Cytometry to Analyze Cryptococcus Infection of Macrophages. *Methods Mol. Biol.* **2017**, *1519*, 349−357.
(51) Wang, J.; King, J. E.; Goldrick, M.; Lowe, M.; Gertler, F. B.; Roberts, I. S. Lamellipodin Is Important for Cell-to-Cell Spread and Actin-Based Motility in Listeria monocytogenes. *Infect. Immun.* **2015**, *83*, 3740−3748.
(52) Proal, A. D.; Inge, A. L.; Trevor, G. M. Microbe-microbe and host-microbe interactions drive microbiome dysbiosis and inflammatory processes. *Discovery Med.* **2017**, *23*, 51−60.
(53) Ireton, K.; Van Ngo, H.; Bhalla, M. Interaction of microbial pathogens with host exocytic pathways. *Cell. Microbiol.* **2018**, *20*, 1−10.
(54) Kocks, C.; Hellio, R.; Gounon, P.; Ohayon, H.; Cossart, P. Polarized distribution of Listeria monocytogenes surface protein ActA at the site of directional actin assembly. *J. Cell Sci.* **1993**, *105* (Pt 3), 699−710.
(55) Welch, M. D.; Rosenblatt, J.; Skoble, J.; Portnoy, D. A.; Mitchison, T. J. Interaction of Human Arp2/3 Complex and the Listeria monocytogenes ActA Protein in Actin Filament Nucleation. *Science* **1998**, *281*, 105−109.
(56) Cohen, R. N.; Rashkin, M. J.; Wen, X.; Szoka, F. C. Molecular motors as drug delivery vehicles. *Drug Discovery Today: Technol.* **2005**, *2*, 111−118, DOI: 10.1016/j.ddtec.2005.04.003.
(57) Dhanda, A. S.; Lulic, K. T.; Yu, C.; Chiu, R. H.; Bukrinsky, M.; Guttman, J. A. Listeria monocytogenes hijacks CD147 to ensure proper membrane protrusion formation and efficient bacterial dissemination. *Cell. Mol. Life Sci.* **2019**, *76*, 4165−4178.
(58) Mandal, M.; Lee, K.-D. Listeriolysin O-liposome-mediated cytosolic delivery of macromolecule antigen in vivo: enhancement of antigen-specific cytotoxic T lymphocyte frequency, activity, and tumor protection. *Biochim. Biophys. Acta, Biomembr.* **2002**, *1563*, 7−17.
(59) Walls, Z. F.; Goodell, S.; Andrews, C. D.; Mathis, J.; Lee, K.-D. Mutants of listeriolysin O for enhanced liposomal delivery of macromolecules. *J. Biotechnol.* **2013**, *164*, 500−502.
(60) Mathew, E.; Hardee, G. E.; Bennett, C. F.; Lee, K.-D. Cytosolic delivery of antisense oligonucleotides by listeriolysin O-containing liposomes. *Gene Ther.* **2003**, *10*, 1105−1115.
(61) Pizarro-Cerdá, J.; Kühbacher, A.; Cossart, P. Entry of Listeria monocytogenes in mammalian epithelial cells: an updated view. *Cold Spring Harbor Perspect. Med.* **2012**, *2*, 1−18.
(62) Czuczman, M. A.; Fattouh, R.; van Rijn, J. M.; Canadien, V.; Osborne, S.; Muise, A. M.; Kuchroo, V. K.; Higgins, D. E.; Brumell, J. H. Listeria monocytogenes exploits efferocytosis to promote cell-to-cell spread. *Nature* **2014**, *509*, 230−234, DOI: 10.1038/nature13168.
(63) Borlace, G. N.; Jones, H. F.; Keep, S. J.; Butler, R. N.; Brooks, D. A. Helicobacter pylori phagosome maturation in primary human macrophages. *Gut Pathog.* **2011**, *3*, No. 3, DOI: 10.1186/1757-4749-3-3.
(64) Shwartz, A.; Goessling, W.; Yin, C. Macrophages in Zebrafish Models of Liver Diseases. *Front. Immunol.* **2019**, *10*, No. 2840, DOI: 10.3389/fimmu.2019.02840.

https://doi.org/10.1021/acsomega.3c10519
ACS Omega 2024, 9, 18260−18272

(65) Palanikumar, L.; Al-Hosani, S.; Kalmouni, M.; Nguyen, V. P.; Ali, L.; Pasricha, R.; Barrera, F. N.; Magzoub, M. pH-responsive high stability polymeric nanoparticles for targeted delivery of anticancer therapeutics. *Commun. Biol.* **2020**, *3*, No. 95, DOI: 10.1038/s42003-020-0817-4.

(66) Zhao, Q.; Shi, M.; Yin, C.; Zhao, Z.; Zhang, J.; Wang, J.; Shen, K.; et al. Dual-Wavelength Photosensitive Nano-in-Micro Scaffold Regulates Innate and Adaptive Immune Responses for Osteogenesis. *Nano-Micro Lett.* **2021**, *13*, No. 28, DOI: 10.1007/s40820-020-00540-z.

https://doi.org/10.1021/acsomega.3c10519
ACS Omega 2024, 9, 18260−18272